Ice nucleation on silicone rubber surfaces differing in roughness parameters and wettability: experimental investigation and machine learning–based predictions

S. Keshavarzi[1*], A. Entezari[2], K. Maghsoudi[1], G. Momen[1], R. Jafari[1]

[1]Department of Applied Sciences, University of Québec in Chicoutimi, Chicoutimi, Québec, Canada

[2] The Hong Kong Polytechnic University, Hong Kong

Corresponding author: Samaneh Keshavarzi,

Email address: samaneh.keshavarzi1@uqac.ca

Abstract

Superhydrophobic surfaces serving as icephobic surfaces are a passive means of limiting the icing of surfaces. Ice nucleation time depends on not only liquid properties and environmental conditions but also surface features; however, it is challenging to investigate ice nucleation time and the influencing parameters simultaneously. This manuscript presents two approaches, experimental testing and machine learning, to study ice nucleation time on exposed surfaces. Hydrophobic/superhydrophobic silicone rubber surfaces were fabricated, and these surfaces varied in their wettability and roughness parameters. Superhydrophobic surfaces characterized by a higher arithmetic average, root mean squared, ten-point height, maximum height of the profile, and a Gaussian roughness distribution—skewness near 0—had longer ice nucleation times. We then used neural networks to model icephobicity in relation to ice nucleation time. The predicted ice nucleation time of the model, trained using some of the experimental results, demonstrated a good agreement with the experimental outcomes. Furthermore, this machine learning approach determined the relative importance of roughness parameters, surface wettability, temperature, and droplet volume in determining surface icephobicity. The proposed approach provides a starting point for studying heterogeneous ice nucleation prediction through an understanding of the key parameters required to optimize the icephobic behavior of superhydrophobic surfaces.

Keywords: heterogeneous nucleation, ice nucleation time, surface roughness parameters, machine learning, superhydrophobic surface, icephobicity

1. Introduction

Ice formation on exposed surfaces is common in cold climates and can represent a health and safety issue as well as affect the optimal performance of infrastructure, including irreversible damage to equipment and marked economic costs [1,2]. Therefore, effective measures are needed to remove accumulated ice or prevent its initial formation. These ice removal strategies can be divided into active and passive approaches. Active approaches involve applying external energy—involving chemical, mechanical, and thermal methods—and are thus often time-consuming, uneconomic, and often environmentally harmful. Passive approaches delay ice formation or reduce ice adhesion without external energy being applied [3–5].

Much recent research has explored the use of superhydrophobic surfaces as icephobic surfaces for delaying freezing time and reducing ice adhesion; these surfaces comprise low surface energy materials and surface roughness. This passive anti-icing/deicing approach is inspired by lotus leaves, and these surfaces are fabricated by creating micro/nanostructures that contain low surface energy chemicals and trapped air within the micro/nanostructures. A correlation between superhydrophobicity and both a reduction in ice adhesion and a delay in ice accretion has been documented in several studies [6–9]. Superhydrophobic surfaces can prevent ice formation on a solid surface by decreasing both contact time and contact area and increasing droplet roll-off. Some investigations, however, have questioned the efficacy of superhydrophobic surfaces for icephobic applications [10,11].

The freezing of a water droplet on a cold surface does not occur immediately upon contact. For all ice formation mechanisms and scenarios, the ice nucleation process represents a

fundamental and crucial step [12]. The ice nucleation process can be divided into homogeneous nucleation and heterogeneous nucleation, which correspond respectively to the absence or presence of external solid surfaces or particles during nucleation [13,14]. In reality, eliminating the role of foreign solid particles (e.g., dust particles, interfaces of nucleating systems) is almost impossible. Furthermore, there is a multitude of factors that can work either in concert or in competition to alter the nucleation process; e.g., environmental conditions, surface characteristics (in the case of heterogeneous icing), the amount of cooling, the degree of purity of the mother phase, droplet size, and the stochastic nature of ice nucleation [15–17]. Hence, understanding the ice nucleation process and its interaction with both surface and environmental characteristics is vital. Although finding a relationship between these various affecting parameters and icephobicity is complex, it is critical for predicting ice nucleation time for application to icephobic surface design and optimization.

Rahimi et al. [18] compared the freezing delay of a water droplet on hydrophilic and hydrophobic substrates having similar surface topographies and found longer freezing delays for droplets on a slightly hydrophilic substrate; thus, ice formation kinetics depend on surface chemistry, as well as surface wettability and topography. In their study of water droplet freezing on hydrophilic, hydrophobic, and superhydrophobic surfaces, Qi et al. [9] observed that the contact angle strongly influenced water droplet freezing time, i.e., a longer freezing time as contact angle increased. Hao et al. [19] prepared five substrates differing in topology and wettability and assessed the ice nucleation and complete freezing time of sessile droplets on smooth, micro-structured, and micro/nanostructured surfaces. Surface roughness significantly influenced ice nucleation time, and they determined that a

smooth surface having a roughness less than that of a critical ice nuclei experiences a longer freezing delay than a superhydrophobic surface with hierarchical structures. However, as reported in [20], sessile droplet freezing on polished (hydrophilic) silicon wafers and cylindrical micro-micro hierarchical (hydrophobic) silicon surfaces showed hierarchical micro-microstructures to produce longer ice nucleation times than hydrophilic surfaces; the hierarchical structure has a surface roughness greater than the critical radius of homogeneous nucleation—according to nucleation theory, ice nuclei must reach a critical radius for ice initiation and growth, a radius that varies with the degree of supercooling. When surface temperature is held constant, differences in ice nucleation onset between hierarchical and polished surfaces stem from differences in surface topologies and determine the dominance of wetting characteristics on ice nucleation [20].

The effect of surface topography on ice nucleation is also unclear. Surface characteristics and possible methods of modifying them to prevent or delay ice formation are critical to understanding how surface conditions influence icing. Altering surface characteristics—by modifying surface properties, surface energy, and roughness—affects surface wettability and the energy barrier to nucleation and, hence, the nucleation rate [18]. Surface roughness, as a measurement of surface texture, cannot be adequately described using a single parameter such as root mean square roughness (S_q) or average surface roughness (S_a). Rather, a set of surface roughness parameters, including ten-point height (S_z), maximum height of the profile (S_t), skewness (S_{sk}), kurtosis (S_{ku}), and autocorrelation length (S_{al}), must be used to accurately evaluate the surface roughness [21–23]. Multiple studies have assessed the influence of roughness parameters on wettability and icing, with some focusing on superhydrophobicity [24–27] and others on icing [28–31]. Bosher et al.

[24] used the nano- and microscale roughness characterization of surfaces to show that substrate surface skewness is the major parameter influencing the water contact angle for identical nano-rough plasma-polymerized PDMS coatings. They concluded that a Gaussian distribution of the roughness height is best for achieving a superhydrophobic surface. Yuan et al. [25], using computer modeling, showed that decreasing skewness and holding kurtosis at around 3 were effective for ensuring droplet bouncing. Yeong et al. [28] investigated the effect of S_a, S_{sk}, S_{ku}, and S_{al} on ice adhesion strength and reported that low S_{al} values led to low ice adhesion, whereas Davis et al. [29] showed a correlation between reduced ice adhesion and a combination of increased hydrophobicity, reduced roughness, increased skewness and kurtosis, and reduced autocorrelation length.

Although surface roughness plays a crucial role in affecting surface wettability and, consequently, the icing-related properties of a surface, there remains an absence of comprehensive studies focused on the relationships between surface wettability, roughness parameters, and ice nucleation time. Therefore, we chose to study five roughness parameters to determine the relationship between roughness parameters, wettability, and ice nucleation time. Nonetheless, analyzing these parameters together is challenging. To illustrate and understand these relationships, we propose and apply a novel machine learning–based model of ice nucleation time. We test five surfaces differing in roughness parameters and wettability to determine the combination of parameters favoring a maximum ice nucleation time.

Experiments in conventional multifactor systems can be conducted by varying one factor at a time. This approach is time-consuming, and interactions among variables may also be ignored, leading to a low efficiency of systems. Another major shortcoming of traditional

approaches relates to highly complex and nonlinear systems that may govern the parameters; it is difficult and sometimes even impossible to present these types of systems using traditional models. Even when a traditional model capable of dealing with these complex systems is developed, it may be impractical for use in prediction [32]. As a possible solution, machine learning techniques have received much attention for their application to complex systems and their capacity to deal with issues of nonlinearity. Machine learning–based approaches can reduce operating costs and improve the speed of data analysis. Machine learning can also identify complex relationships between independent and dependent variables through nonlinear data processing [33–35]. Ringdahl et al. [36] applied molecular dynamics simulations and machine learning to study ice adhesion strength on rough surfaces. It was the first time machine learning was applied to anti-icing surface design and showed encouraging predictions. Ramachandran [37] developed machine learning models to optimize the icephobicity of concrete by using artificial neural networks to predict surface ice adhesion strength and the coefficient of restitution of water droplets bouncing off the surface under freezing conditions. Fitzner et al. [38] developed a data-driven machine learning–based approach to identify descriptors for heterogeneous ice nucleation as a means of increasing the quantitative understanding of heterogeneous ice nucleation. However, despite these advances, no existing research has reported using machine learning to predict ice nucleation time.

The main objective of our study is to determine the optimal surface characteristics to enhance anti-icing properties of surfaces through analysis of the ice nucleation of water droplets deposited onto solid hydrophobic to superhydrophobic surfaces. By analyzing the freezing of water droplets on the solid surface, we also investigate how surface

characteristics, including surface wettability, surface roughness (S_a, S_q, S_z, S_t, and S_{sk}), droplet volume, and surface temperature, affect the ice nucleation process. Exploring these associated parameters represents a significant step for designing icephobic surfaces. We exploit the machine learning approach to investigate multiple variables affecting the icephobic behavior of surfaces, i.e., ice nucleation time, observe interactions between parameters, identify the most important factors (surface wettability, surface roughness (S_a, S_q, S_z, S_t, and S_{sk}), droplet volume, and surface temperature) affecting ice nucleation time, and develop a prediction tool for ice nucleation time as a function of the influencing parameters.

2. Material and Methods

2.1. Sample Preparation

The required surface micro-nanostructures were created on high-temperature vulcanized (HTV) silicone surfaces via direct replication from a series of aluminum (A6061-T6) templates. The template patterns were fabricated using a chemical-etching method. The templates were immersed in a hydrochloric acid solution of varying concentrations: 4.8, 9.8, 14.8, 19.8 wt.% for 2 h to produce different surfaces [39]. A press machine (Carver, USA) having a maximum clamp force capacity of 194 kN was used to replicate the template patterns on the silicone rubber surfaces under the following molding parameters: a molding pressure of 35 MPa, a curing time of 4.7 min, and a mold temperature of 149 °C. Once the rubber was cured, the molds were opened, and the cured rubber was removed from the three-piece flat mold cavity (Fig. 1). No subsequent processing was carried out on the silicone rubber surfaces prior to the freezing tests.

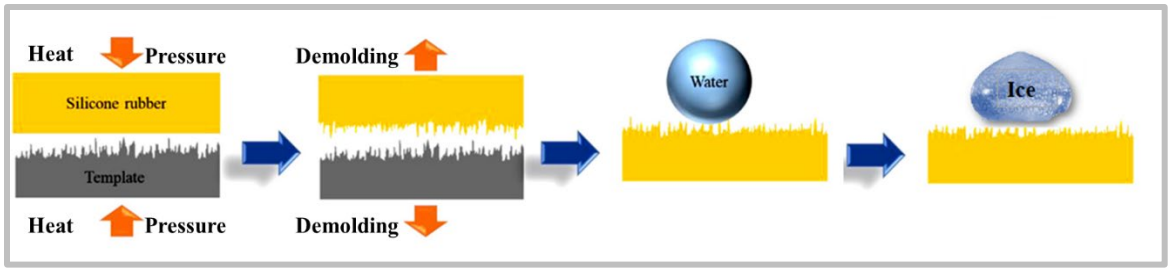

Fig. 1. Schematic of the fabrication of micro-nanostructured silicone rubber surfaces via a microcompression molding technique [40]

2.2. Surface Characterization

A Kruss™ DSA100 goniometer at 25 °C ± 0.5 °C determined the contact angle (CA) of a 4 uL deionized water droplet on the produced surfaces. In addition, to avoid condensation affecting the measurements, anhydrous calcium sulfate desiccants (Indicating DRIERITE impregnated with cobalt chloride) were used. Contact angle hysteresis (CAH) was calculated as the difference between the advancing and receding CAs of the moving water droplet on the surface. To ensure reproducibility and accuracy, we repeated each measurement at five points across each surface. The surface roughness parameters and the 3D profiles of the surfaces were obtained using a confocal laser microscopy profiler (Profil3D, Filmetrics, USA). Detailed measurement settings can be found in Table 1. To obtain the surface roughness, Fill In Invalids and Flatten filters used for data pre-processing. The morphology of fabricated surfaces was observed using a scanning electron microscope (SEM, JSM-6480 LV by JEOL Japan).

Table 1. Surface measurement parameters.

Parameter	Unit	Value
Magnification	-	50×
Area size	μm^2	386.3 × 339.3
Estimated vertical resolution	nm	56
Lateral sampling intervals	µm	0.176

188

189 *2.3. Experimental Setup*

190 We studied the ice nucleation of a single water droplet on hydrophobic/superhydrophobic
191 silicone rubber surfaces using an experimental freezing setup that included a thermally
192 insulating and optically transparent chamber, high-speed camera, thermostatic bath, cold
193 base, drop injection system, test samples, data acquisition system, temperature sensor,
194 humidity sensor, and a vibration-free table (Fig. 2). A thermally insulating and optically
195 transparent double-layer chamber was used to ensure that the parameters affecting ice
196 nucleation were uniform during experiments to increase the accuracy and reproducibility
197 of the experiments. Its transparency facilitates imaging of the freezing droplet. The
198 temperature of the cold base was adjusted using the thermostatic bath. Temperature and
199 humidity sensors monitored the chamber temperature and humidity. A high-speed camera
200 (MotionBLITZ, MIKROTRON, EoSens Cube 7, Germany) and LED illuminator were
201 used to visually record the experimental outcome.

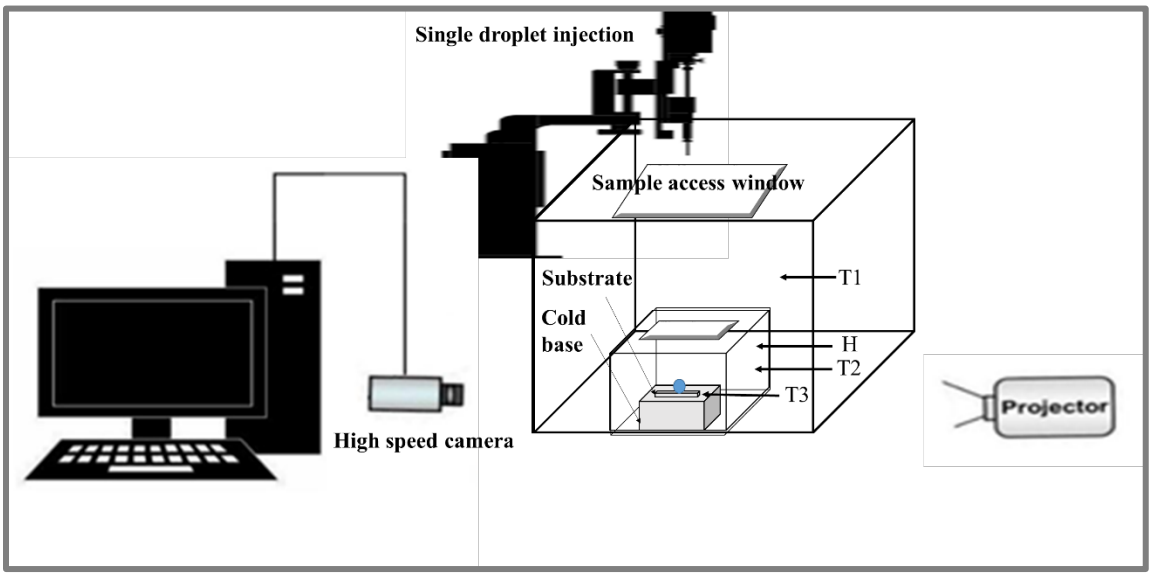

202

Fig. 2. Schematic of the experimental setup for the ice nucleation study (H = humidity of small chamber (%), T1 = large chamber temperature (°C), T2 = small chamber temperature (°C), T3 = cold base temperature (°C)).

Temperature and humidity of the surrounding environment and chamber were recorded before the experimental tests. The temperature and the relative humidity of the chamber were set at 20 °C and 35% ± 3%, respectively. The cold base temperature was then decreased to temperatures of −10 and −20 °C, and the silicone rubber sample was placed on the cold plate. Once sample temperature was stable (prior to experimentation, the temperature of the surface was measured with an IR camera and a thermocouple (K-type) which was removed during the experiments), a droplet (either 10 or 20 µL) was placed onto the cold surface with no frost formation, and its freezing process was recorded using the high-speed camera. For each test, two steps in the freezing of droplets were identified. The first step, defined as nucleation time, represented the moment from when the droplet was placed onto the surface until the rapid recalescent stage. This stage can be easily monitored using a high-speed camera at 1000 frames per second. This step was followed by the complete freezing step. The reported nucleation times are the average of 10 experimental runs.

3. Results and Discussion

3.1. Surface Characterization

Table 2 shows the wettability properties of each sample along with the surface roughness parameters, and Fig. 3 illustrates various surface structures using SEM images and 3D profiles. Standard surface roughness parameters including S_a (the average surface roughness) and S_q (the root mean square roughness) are generally used to evaluate surface roughness; however, these two values are unable to adequately describe the surface

roughness, as they relate only to vertical height and provide no description of horizontal surface features. Relying on only these two parameters can produce very similar roughness values despite very different surface morphologies, and the reverse is also true [41]. To determine those parameters best describing the icephobicity of silicone rubber surfaces, we relied on a combination of commonly used roughness parameters (S_a and S_q) and some less common parameters (S_z (ten-point height), S_t (maximum height of the profile), and S_{sk} (skewness)). Understanding more topographical characterization parameters can help in design of icephobic surfaces to offer the optimum surface characteristics to enhance anti-icing properties of surfaces can be considered as one of the highly important issues. In our current study, the main shortcoming is the limited number of roughness parameters that we used.

Sample 1 was a hydrophobic surface (CA ~116° and CAH ~46.5°) replicated from a smooth aluminum template. Therefore, the hydrophobic property of Sample 1 stemmed solely from the intrinsic hydrophobicity of the silicone rubber. The surface roughness of the other prepared samples differed markedly from that of Sample 1 (Table 2); for example, the root mean squared (S_q) of Samples 2, 3, 4, and 5 increased about 1.87, 3.77, 4.49, and 4.28× that of Sample 1. This combination of elevated surface roughness and surface hydrophobicity of the silicone rubber produced the superhydrophobic properties observed for samples 2–5. In addition to S_q, both S_z and S_t testify to the created surface profiles being characterized by relatively high peaks and deep valleys. It is also noteworthy that the skewness value (as an indicator of the asymmetry of the profile about the mean plane) varied between −0.37 and 0.43.

Table 2. Water contact angle (CA), contact angle hysteresis (CAH), and 3D roughness values of the produced surfaces at 25 °C ± 0.5 °C and a relative humidity of about 25%

Sample No.	CA (°)	CAH (°)	S_a (µm)	S_q (µm)	S_z (µm)	S_t (µm)	S_{sk}
1	116.0 ± 2	46.5 ± 2.4	1.46	1.76	3.74	3.6	0.28
2	154.5 ± 1.4	28 ± 1.6	2.13	3.29	14.21	18.4	0.31
3	165.3 ± 1.1	1.5 ± 0.2	5.21	6.64	21.65	24.86	0.43
4	166.6 ± 0.9	0.6 ± 0.3	6.49	7.9	33.67	39.97	0.18
5	162.8 ± 0.8	1.3 ± 0.8	6.03	7.54	28.54	33.99	−0.37

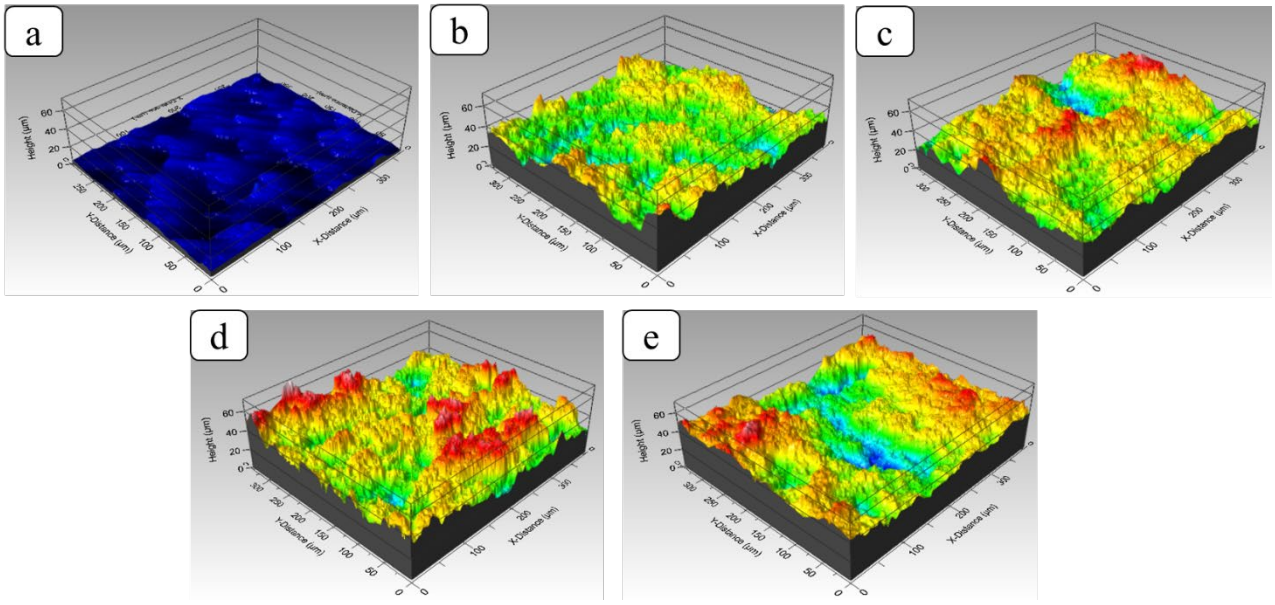

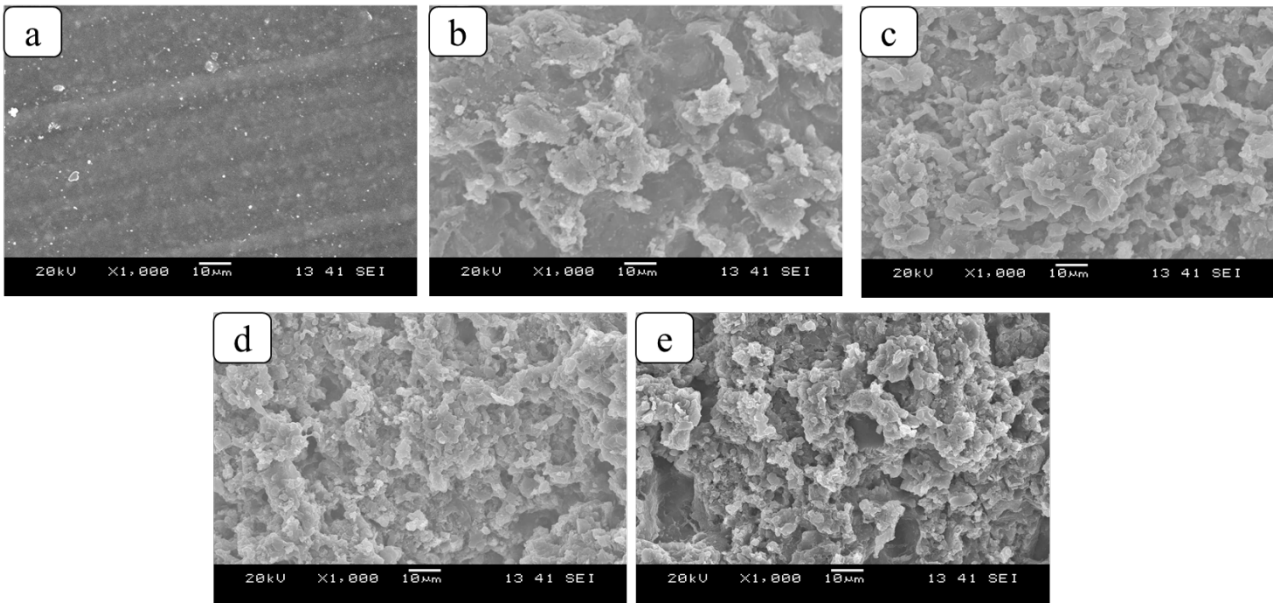

Fig. 3. The 3D surface profiles and SEM images of samples (a) 1, (b) 2, (c) 3, (d) 4, and (e) 5

3.2. The Effect of Surface Wettability and Roughness

Ice nucleation, formation, and freezing delay can be affected markedly by surface characteristics such as surface wettability, roughness, and surface chemistry [42–45]. Establishing the relationships between surface roughness and wettability and the ice nucleation process represents a problem in the design of icephobic surfaces. To determine these complex correlations among surfaces features and ice nucleation time, we investigated the ice nucleation process of sessile droplets on cold surfaces of differing wettability and roughness (Table 2). Fig. 4 shows the shape of water droplets at various times during freezing on the five surfaces. It is also worth mentioning that the contact angle measurement in Table 2 was at 25 °C ± 0.5 °C and RH = 25% while the figure 4 was at −10 °C and RH = 35 %. Therefore, the contact angles of the droplets shown in Fig. 4 do not match the contact angle information in Table 2. Calculated cooling time is also provided in supplementary file section 1.

269

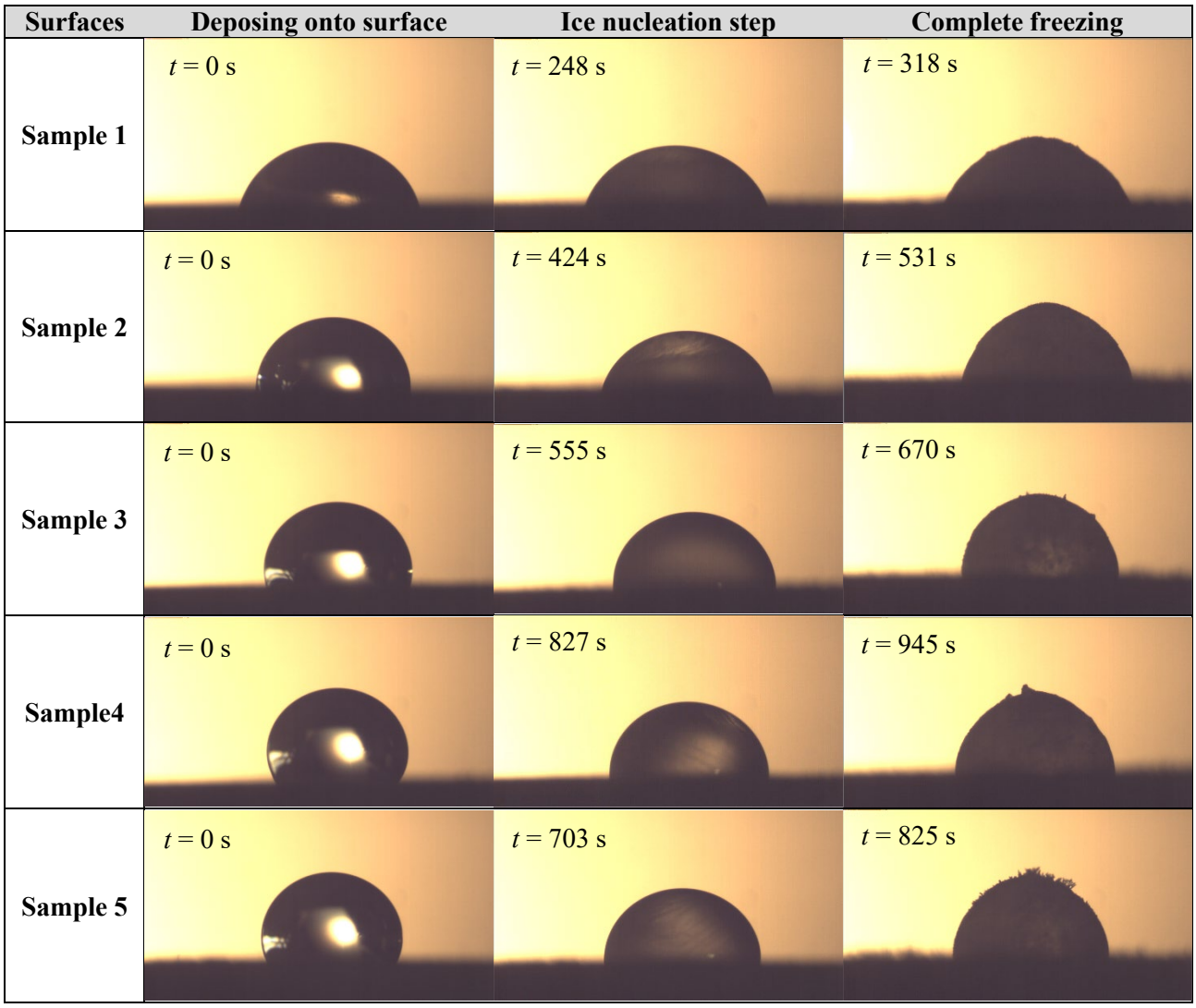

Fig. 4. Images of the freezing of a 10 µL droplet on different solid surfaces at −10 °C

Ice nucleation times for 10 µL droplets placed onto these five substrates at −10 °C varied markedly (Fig. 5). Sample 1, the unaltered silicone rubber, had an ice nucleation time of 248 s, whereas this increased to 424 s for Sample 2 (CA ~154.5° and CAH ~28°) and to 827 s for Sample 4 when the CA and surface roughness were 166.6° and 7.9 µm, respectively, and CAH decreased to 0.6°. The slight decrease in CA and roughness and an increase in CAH of Sample 5, relative to Sample 4, produced a decrease in ice nucleation time to 703 s. Similar trends were observed at different temperatures and droplet volumes (Fig. 5). The roughest surface (Sample 4) offered the longest nucleation time, as more air

was trapped in the interface between the rough surface and the water droplet. The trapped air acts as a thermal insulator and reduces heat transfer between the droplet and the solid substrate.

Classical nucleation theory [46,47] holds that two main parameters affect the critical energy barrier of heterogeneous nucleation: ΔT_m, which relates to the degree of supercooling, and f, the interfacial correlation factor (Eq. 1). The latter parameter is a function of the roughness radius of curvature (R) and the CA between the ice nucleus and the surface structure (θ_{iw}).

$$\Delta G^*_{WI} = \frac{16\pi {\sigma_{WI}}^3 \vartheta_I^2}{3\left[\Delta h_{WI}\left(\Delta T_m / T_m\right)\right]^2} f(R, \theta_{iw}) , \quad (1)$$

where Δh_{WI}, T_m, σ_{WI}, and ϑ_I are the enthalpy of melting, melting point temperature, the interfacial ice-water tension, and the molar volume of the solid phase, respectively.

When the radius of the curvature of a solid particle or surface texture is much greater than the critical radius of homogeneous nucleation, f depends only on the ice-water contact angle [48]. In this study the surface curvature effect of heterogeneous nucleation theory was not considered. The experiments do not investigate the curvature effect and the results can be interpreted without this effect.

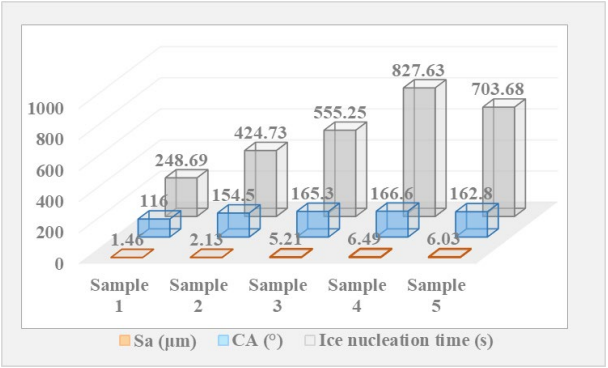

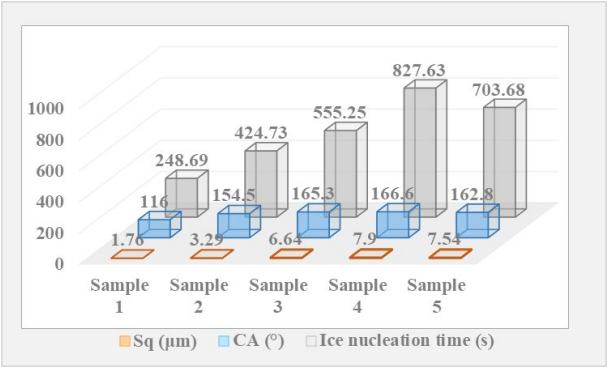

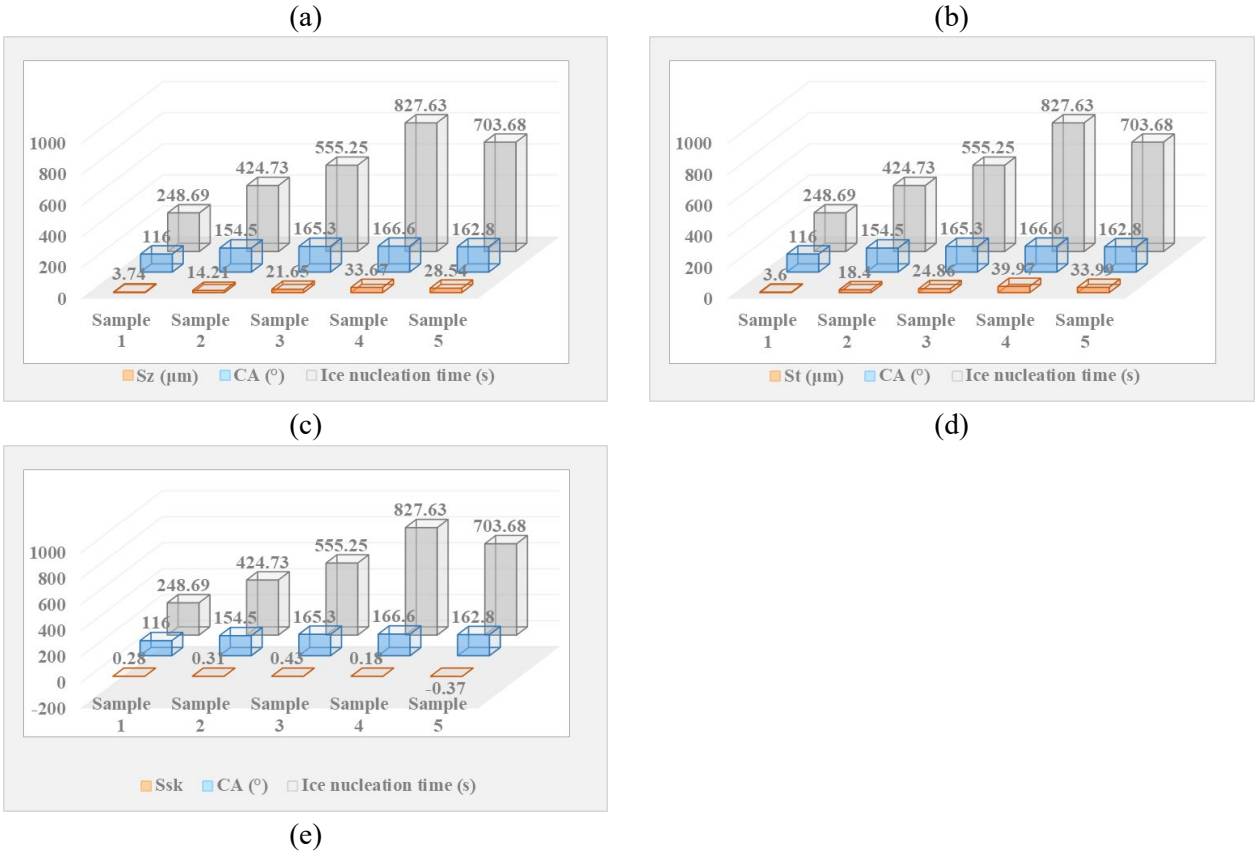

Fig. 5. Ice nucleation times for a 10 µL droplet on different surfaces as a function of CA and (a) S_a, (b) S_q, (c) S_z, (d) S_t, and (e) S_{sk} at −10 °C

We observed a significant increase in ice nucleation time as CA increased and CAH decreased because of the reduced contact area and presence of air pockets within the surface microstructures. It means that wetting characteristics of our samples has a strong effect on the ice nucleation time as the greater the CA, the longer freezing delay time. The superhydrophobic surfaces had a smaller contact area between the water droplet and substrate. A smaller contact area, therefore, can lead to a relatively low heterogeneous nucleation rate from classical nucleation theory.

To illustrate how surface roughness affects ice nucleation time, we can plot ice nucleation time and CA against five common surface roughness parameters (S_a, S_q, S_z, S_t, and S_{sk}) (Fig. 5). The clear relationship between the ice nucleation time and CA and both S_a and S_q

306 demonstrates that a marked microstructure height prevented the droplet from touching the
307 base of the microstructures. The same conclusion can also be drawn when evaluating the
308 relationship between ice nucleation time, CA and both S_z and S_t.

309 On the pristine silicone rubber surface, roughness parameters were $S_a = 1.46$ µm, $S_q =$
310 1.76 µm, $S_z = 3.74$ µm, and $S_t = 3.6$ µm. The parameters describing microstructure
311 height demonstrated a significant influence on surface wettability and ice nucleation time.
312 The increase in CA and ice nucleation time for the superhydrophobic surfaces (Samples 2–
313 5) can be explained by increased S_a, S_q, S_z, and S_t. Furthermore, the three superhydrophobic
314 surfaces having a CAH <10° (samples 3–5) showed considerably higher S_a, S_q, S_z, and S_t
315 than those of the superhydrophobic silicone rubber having a CAH >10° (Sample 2). Greater
316 roughness increased the CA, in accordance with Cassie-Baxter wetting models, where
317 surface roughness directly influences the wetting state (samples 3–5).

318 As S_a, S_q, S_z, and S_t of these silicone rubber surfaces increased, a greater number of grooves
319 were apparent underneath the droplet. A droplet on a rough surface having larger S_a, S_q,
320 S_z, and S_t values would have a smaller liquid–solid contact area and, therefore, a longer ice
321 nucleation time. If S_a, S_q, S_z, and S_t are not large enough, liquid can penetrate the grooves,
322 and the droplet remains in a Wenzel state where the ice–solid contact area is greater.

323 Surface skewness values were between −0.5 and 0.5 (Fig. 5); therefore, the height
324 distribution of all surfaces was highly symmetrical and minimally skewed. The optimal
325 performance in terms of a long ice nucleation time and high CA were obtained for a surface
326 with S_{sk} close to zero. Regardless of whether there was a lower S_{sk}, corresponding to more
327 valleys or a greater S_{sk}, corresponding to more peaks, CA decreased. Therefore, surfaces
328 having a Gaussian distribution of roughness were more likely to be superhydrophobic and

329 icephobic with longer freezing delay times. Sample 4 had the longest freezing delay time
330 (827.63 s) and a near-zero S_{sk} (0.18).

331 Therefore, the ice nucleation times correlated well with the roughness parameters. Very
332 rough surfaces dominated by peaks should show better water repellency (higher CA and
333 lower CAH) and greater icephobicity in terms of a longer ice nucleation time. Nonetheless,
334 it remained uncertain which specific roughness parameters were best correlated with
335 surface hydrophobicity/superhydrophobicity and icephobicity. We therefore used machine
336 learning to identify these parameters (Section 3.5).

337 *3.3. The Effect of Surface Temperature*

338 The measured ice nucleation times were plotted (Fig. 5) to investigate the relationship
339 between the ice nucleation time and surface temperature. According to average values of
340 ice nucleation time (Fig. 6), as surface temperature decreased from −10 to −20 °C, the
341 shortest ice nucleation time dropped from 248.69 to 80.38 s for a 10 μL water droplet
342 (observed on Sample 1) and the longest nucleation time dropped from 827.63 to 345.60 s
343 (observed on Sample 4). Classical nucleation theory best explains this tendency of shorter
344 ice nucleation times at lower temperatures. This theory posits that the critical energy barrier
345 of nucleation is inversely proportional with the square of supercooling ($\Delta {T_m}^2$) and
346 therefore decreases with an increase in the degree of supercooling (decrease in governing
347 temperature, T) (Eq. 1) [18].

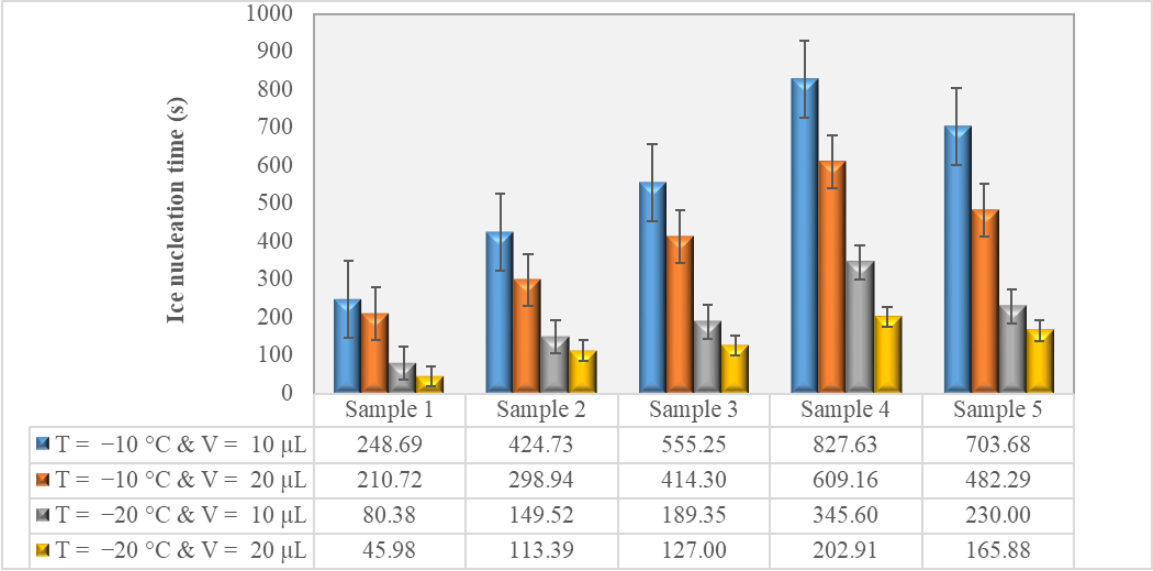

	Sample 1	Sample 2	Sample 3	Sample 4	Sample 5
T = −10 °C & V = 10 µL	248.69	424.73	555.25	827.63	703.68
T = −10 °C & V = 20 µL	210.72	298.94	414.30	609.16	482.29
T = −20 °C & V = 10 µL	80.38	149.52	189.35	345.60	230.00
T = −20 °C & V = 20 µL	45.98	113.39	127.00	202.91	165.88

Fig. 6. Comparison of ice nucleation times of 10 µL and 20 µL water droplets on the various silicone rubber surfaces at −10 °C and −20 °C

3.4. The Effect of Droplet Size

The icing on surfaces characterized by different surface structures (from hydrophobic to superhydrophobic) was then tested, focusing on the effect of droplet volume at two temperatures. As droplet volume increased, ice nucleation time markedly decreased (Fig. 6). According to classical nucleation theory, ice nucleation is dominated by the most active nucleation site above the critical radius. The probability of nucleation appears less likely for smaller drops because of their smaller volume [48]. Zhang et al. [49] experimentally and statistically analyzed the effect of droplet size and nucleation time on the nucleation temperatures of water droplets (1, 5, and 10 µL) placed on a cold horizontal aluminum plate. They observed that nucleation temperature decreased (and the standard deviation increased) as droplet volume decreased. Moreover, larger droplets had a higher nucleation rate with lower nucleation temperatures. Smaller droplets have a lower nucleation temperature because there are fewer critical nuclei inside the droplet and at the solid–liquid or gas–liquid interface than within a larger droplet.

Furthermore, the possibility of freezing can be estimated using the nucleation rate of a single embryo, a rate which is inversely proportional to the delay time of ice nucleation and is based on the kinetic theory. The nucleation rate of ice embryos (I) can be estimated using the equation of Becker and Doring that estimates the rate of ice nucleation per unit time and surface area in relation to the free energy barrier of nucleation of critical embryo [50–52]:

$$I \approx I_0 \exp\left(\frac{-\Delta G^*}{k_B T}\right), \quad (2)$$

where I is the embryo formation rate, I_0 is the kinetic constant, k_B is the Boltzmann constant, and ΔG^* is the critical energy barrier according to Eq. 1 [53].

$$I = 1/(t_{nucleation} A), \quad (3)$$

where A is the contact area which is in relation to the volume V via the water contact angle to air [54] :

$$A = \frac{(9\pi V^2)^{\frac{1}{3}} sin^2\theta}{((2+\cos\theta)(-1+\cos\theta)^2)^{\frac{2}{3}}}, \quad (4)$$

This equation indicates that larger droplets produce shorter freezing delay times at a constant nucleation rate, and our results validate this explanation. For example, at −10 °C for Sample 1, the ice nucleation time was 248.69 s for a 10 µL water droplet, whereas ice nucleation occurred at 210.72 s for a 20 µL droplet (Fig. 6). In contrast, the ice nucleation times at −10 °C for 10 µL and 20 µL water droplets on the rougher surfaces (Samples 2–5) were longer, and ice nucleation times for a 10 µL droplet was always greater than for a 20 µL droplet on the same surface (Fig. 6). A similar pattern was observed for droplets on

the −20 °C surfaces. It should be noted that the magnitude of differences in ice nucleation times at the different temperatures was much greater for the roughened samples than for Sample 1.

3.5. Machine Learning

3.5.1. Model Development

The above investigations showed that a longer ice nucleation time on these silicone rubber surfaces can be achieved by decreasing droplet volume, and increasing the surface roughness parameters to also obtain a Gaussian height distribution. However, to measure the correlation between these parameters, we tested the performance of machine learning models. Machine learning can construct a nonlinear mapping of ice nucleation time and the operating conditions (e.g., surface wettability, roughness, temperature, and droplet volume), using limited experimental data (200 data points), to then predict ice nucleation times and the corresponding operating conditions.

Machine learning models are often based on supervised learning, where models are trained to predict true labels of a training data set and are then evaluated against a test set. There are several traditional machine learning methods, including linear regression, artificial neural networks (ANN), nearest neighbors, support vector machines, and random forest (RF) models. Models of linear regression are intuitive, easy to understand, and can be performed using linear algebra; this results in clear and concise mathematical formulas. Nonetheless, linear regression may not be applicable to data sets having a high degree of nonlinearity. Overfitting issues in linear regression models are generally not detected or resolved by commercially available software. ANNs, on the other hand, do not produce simple correlation formulas, although they do outperform linear regression models when

dealing with nonlinearity within data sets. Unfortunately, overfitting problems can also occur in ANN models . In addition, ANN performance decreases as the nonlinearity of the model increases.

As a branch of deep learning, deep neural network (DNN) models are powerful tools used primarily in computer vision, voice recognition, pattern recognition, and language processing. As with other neural network approaches, DNN includes three primary components in its core: input layer(s), hidden layer(s), and the output layer(s). ANNs and DNNs differ primarily in their number and type of hidden layers, where each layer's output becomes the input for the next layer [55]. Fig. 7 shows a DNN having three hidden layers. In each hidden layer, there are several nodes and an activation function. Although different activation functions can be used, one activation function is generally used for all neurons within a layer (see Section 2 of the Supplemenatry material for more technical details). The input layer consists of T (temperature), V (volume), CA, CAH, S_a, S_q, S_z, S_t, and S_{sk}, with ice nucleation time as the output.

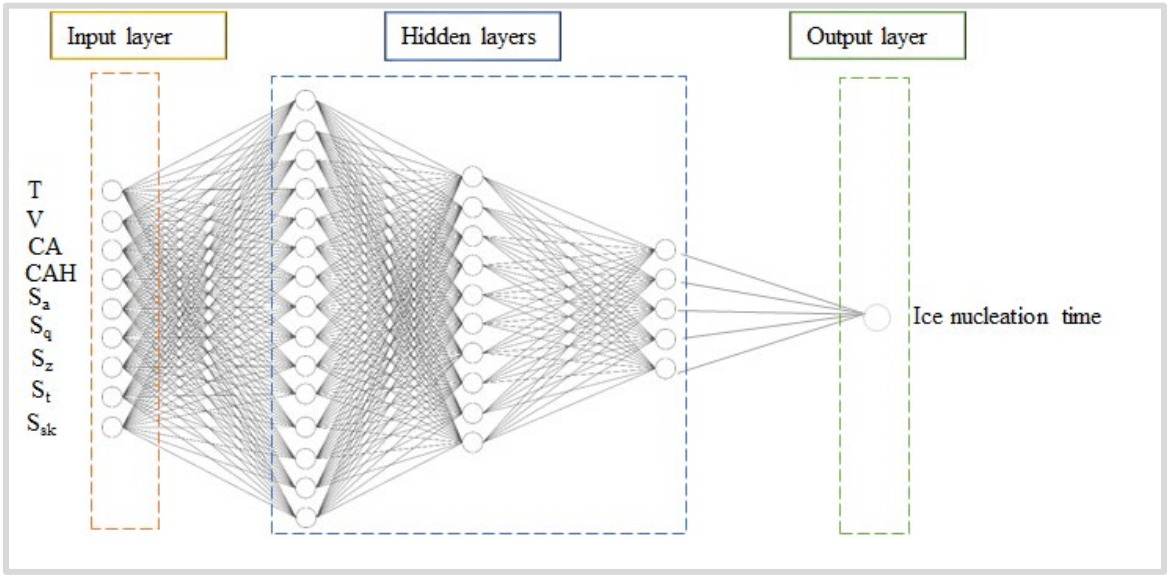

Fig. 7. An example of a deep neural network (DNN) with three hidden layers; temperature (T = −10 and −20 °C), droplet volume (V = 10 and 20 µL), contact angle (CA), contact angle hysteresis (CAH), the root mean square roughness (S_q,), the average surface roughness (S_a), ten-point height (S_z), maximum height of the profile (S_t), skewness (S_{sk}) (Table 2 data)

For creating and assessing the DNN models, the online Python code of Asghari et al. [56] was used. The mean squared error (MSE) of the prediction for the output variable was determined using Eq.5,

$$MSE = \frac{1}{m}\sum_{i}^{m}(\hat{y}_i - y_i)^2. \quad (5)$$

MSE must be smaller than the variance of the output variable for a valid prediction model. Making predictions can be difficult when (1) the variance problem occurs, where a model performs slightly better than the base model, and (2) the overfitting problem, which occurs when a model performs well for the training set but poorly for other data sets (e.g., test or cross-validation data sets). When there are sufficient hidden layers and nodes, it is possible to create a model having no errors for a training data set, although the model will perform poorly when applied to any other data set. A successful DNN model commonly has the data set divided into three pieces at a 70:15:15 distribution. The middle set (called the cross-validation set) compares the performance between the various candidate models. In the end, the performance of the chosen optimal model is reported with respect to the final data set (test set). The error and variance error must be small in a properly constructed model.

In this study, the data set was sliced into three parts, with 70:15:15 portions for the training, cross-validation, and test data sets, respectively. The bias error and variance error of a model should be low. There are several hyperparameters that DNN requires to be

444 implemented, such as types of layers, number of layers, number of nodes in each layer,
445 activation functions for each layer, cost function, an optimization algorithm, and a learning
446 rate. Selecting the values for some of these hyperparameters of DNN is not an exact
447 science; they are mainly determined by the modeler's experience. The hyperparameters of
448 DNN used in this study and their corresponding values are summarized in Table 3. A linear
449 activation function is considered for the final layer, as the aim of this study is to predict ice
450 nucleation time as a regression problem. For the first and hidden layers, Tanh and Relu
451 activation functions were utilized, respectively. For the cost functions, the MSE of the
452 predictions was used. The Adam optimizer was also applied for optimization, and
453 optimization stopped when the cost's variation (reduction) fell to less than 1% of the
454 variance of the output variables of the previous 50 steps.

455 **Table 3.** Hyperparameters of a DNN structure

Hyperparameters	**Status**
Type of layers	Fully connected layers
Input layer activation function	tanh
Hidden layers activation function	relu
Output layer activation function	linear
Optimizer	Adam
Cost function	MSE (mean squared error)
Minimum delta and patience	0.01 σ^2, 50
Epoch	500
Batch size	16
Slicing proportions	70:15:15
Number of hidden layers and nodes	To be decided in the following steps
Weight regularization parameter and type	To be decided in the following steps
Learning rate	0.0001 (the default value of KERAS)

456 Input variables in data sets vary in order of magnitude and range. As this can lower the
457 efficiency of the optimization, features were scaled to an interval of [0, 1] through Eq. 6:

$$y(x_i) = \frac{x_i - min_x}{max_x - min_x}. \quad (6)$$

458

459 *3.5.2. Model Results*

460 The training of machine models requires a massive amount of data. However, by carefully
461 designing the network architecture, training can function using small- to medium-sized
462 data sets. High-performance models can be generated by an efficient search of these
463 developed architectures. Moreover, by reducing the number of neurons in the network and
464 pruning connections within the network, this grow-and-prune can boost model
465 performance and reduce computational costs of the inference process [57]. The produced
466 correlation coefficients were strong (Table 4) and confirmed the use of DNN to assess and
467 predict ice nucleation time from various roughness parameters and wettability.

468 In the model development process, no overfitting was observed, as the error of the cross-
469 validation set and training set were quite similar. Because the model prediction error was
470 less than the output variables' variance, there was no variance problem. Moreover, there
471 was a good correlation between the predicted and actual values of the output variables (Fig.
472 8). In addition, the error percentage of prediction did not show any trends (Fig. 9).

473 **Table 4.** The developed model performance and the cost functions on training, cross-validation,
474 and test data sets, MSE (Mean of squared error), MAE (Mean of absolute error), and MAPE
475 (Mean of absolute percent error)

	CorrCoef	R^2	MSE	MAE	MAPE
DNN-Ensemble-OnTrain	0.996628	0.993267	375.4751	14.42525	6.887508
DNN-Ensemble-OnCV	0.996795	0.9936	333.9455	13.51721	5.933723
DNN-Ensemble-OnTest	0.995501	0.991022	407.1518	16.49789	8.012416
DNN-Ensemble-OnCVTest	0.994723	0.989474	518.7683	18.77193	8.352949

476

477

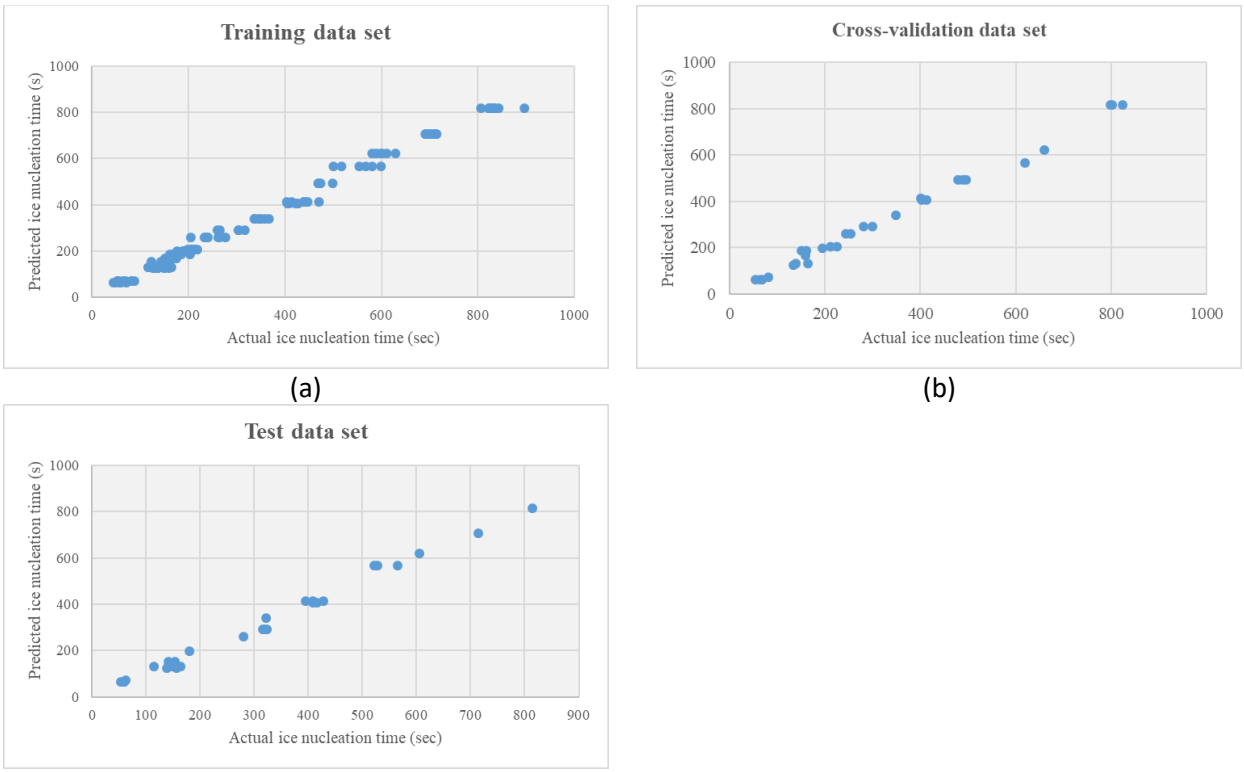

478 **Fig. 8.** Predicted and actual values of the a) training, b) cross-validation, and c) test data set

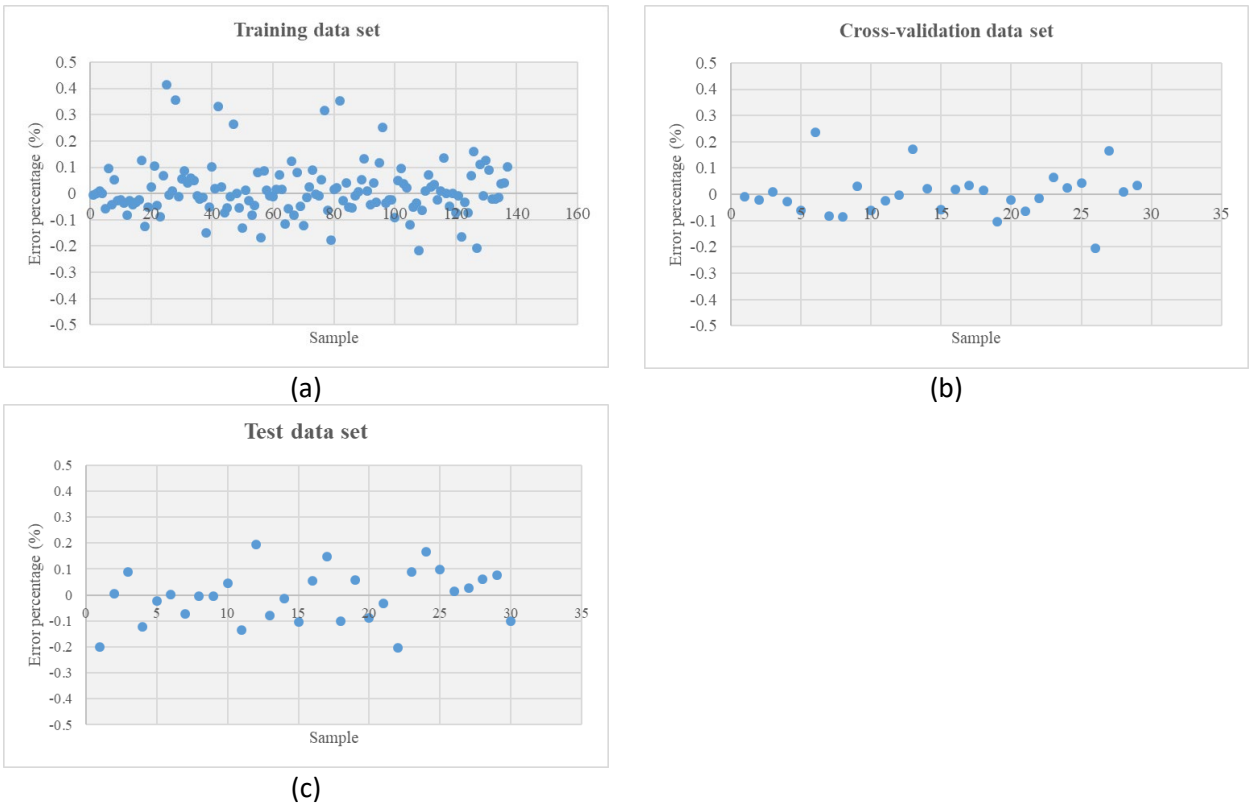

Fig. 9. Error of prediction (%) for the (a) training, (b) cross-validation, and c) test data sets.

As presented in Section 3.2, changes in surface roughness parameters increase the ice nucleation time. To investigate correlation coefficients between variables, a cross correlation matrix was used (see Section 3 of the Supplementary material for more technical details). It remained uncertain from our experimental stage which roughness parameters were most closely correlated with surface hydrophobicity and icephobicity. A machine learning approach can address this issue, however, by analyzing the relative importance of features. Although DNN models have been called black boxes, methods do exist to better understand machine learning models, including DNN models. Game theory was applied to machine learning models by Lunderberg and Lee [58], who proposed SHapley Additive exPlanations (SHAP). Considering each input variable to be a player and the prediction to be a game, they showed how each input variable played a part in every prediction. Therefore, SHAP values reflect the relative importance of each input variable to a DNN regression model.

When the average absolute SHAP value for all input variables was plotted, we observed that T, S_z, V, S_t, CA, CAH, S_{sk}, S_a, and S_q were the most important parameters affecting ice nucleation time (Fig. 10). From classical nucleation theory (Eq. 1–3), the nucleation rate relates to the degree of supercooling, droplet volume, roughness radius of curvature (R), and the CA between the ice nucleus and the surface structure (θ_{iw}). Looking specifically at the inverse relationship of the critical energy barrier of nucleation to the square of supercooling, temperature dependence of droplet properties, and wetting properties, we observed that the effect of temperature on ice nucleation rate dominated, as confirmed by our machine learning approach. In terms of the effect of surface roughness

and wetting state on ice nucleation, S_z was predicted as the most important of the various surface roughness parameters, whereas S_a and S_q have generally been the only surface roughness parameters considered to have an effect on ice nucleation [9,18,19]. Our findings are promising, as for the first time, the impact of the physical parameters of a water droplet (e.g., volume), environmental conditions (e.g., temperature), surface wettability (i.e., CA and CAH), and several surface roughness parameters (i.e., S_a, S_q, S_t, S_z, and S_{sk}) on the icephobicity of hydrophobic/superhydrophobic surfaces were compared and illustrated simultaneously.

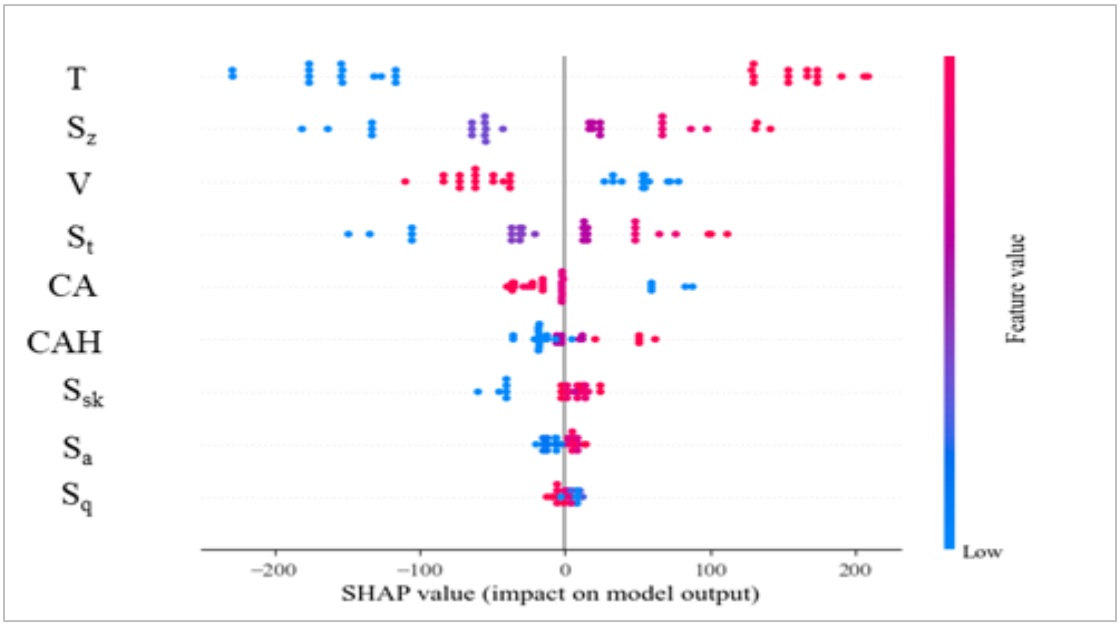

Fig. 10. Importance analysis of the studied features; temperature (T), droplet volume (V), contact angle (CA), contact angle hysteresis (CAH), the root mean square roughness (S_q), the average surface roughness (S_a), ten-point height (S_z), maximum height of the profile (S_t), and skewness (S_{sk})

4. Conclusion

In this study, we successfully accomplished our two main objectives. First, we determined the ability of hydrophobic/superhydrophobic silicone rubber surfaces to increase the ice nucleation time. Five substrates having various roughness parameters and wettability were

519 fabricated. We detailed the relationships between surface wettability, roughness
520 parameters, surface temperature, water droplet size, and ice nucleation time. As substrate
521 temperature decreased and droplet volume increased, the freezing delay was reduced for
522 all five surfaces. Thus, S_a, S_q, S_z, S_t, and S_{sk} parameters can be used to determine surface
523 texturing, where higher S_a, S_q, S_z, and S_t values and a S_{sk} value close to 0 (i.e., a Gaussian
524 distribution for roughness height) lead to superhydrophobic surfaces having a CAH <10º
525 and longer ice nucleation time.

526 The second objective was to accurately predict ice nucleation time. A new machine
527 learning–based approach was proposed and used to model ice nucleation time on the
528 prepared hydrophobic/superhydrophobic silicone rubber surfaces. Using a neural network
529 approach, we developed a model to reliably predict ice nucleation time. Moreover, to
530 understand the roughness parameter that best determines surface icephobicity, we
531 investigated the relative importance of a range of features (T, V, CA, CAH, S_a, S_q, S_z, S_t,
532 and S_{sk}). T, S_z, and V were the most important factors determining ice nucleation time.
533 This study demonstrated an increased ice nucleation time on superhydrophobic surfaces
534 and produced a promising machine learning–based approach for predicting ice nucleation
535 time on surfaces.

536 **CRediT authorship contribution statement**

537 **S. Keshavarzi**: Conceptualization, Investigation, Methodology, Validation, Writing –
538 original draft, Writing - review & editing. **A. Entezari**: Conceptualization, Methodology,
539 Software, Validation, Investigation, Writing - original draft, Writing - review & editing.
540 **K. Maghsoudi**: Conceptualization, Methodology, Software, Validation, Investigation,
541 Writing - original draft, Writing - review & editing. **G. Momen**: Conceptualization, Project

administration, Supervision, Resources, Funding acquisition, Writing - review & editing. **R. Jafari**: Conceptualization, Project administration, Supervision, Resources, Funding acquisition, Writing - review & editing.

Declaration of Conflict of Interest

The authors declare that they have no known competing financial interests or personal relationships that could have appeared to influence the work reported in this paper.

Acknowledgments

The authors would like to acknowledge the financial support from Natural Sciences and Engineering Research Council of Canada (NSERC). We also thank Carol Mercier at the Anti-icing Materials International Laboratory (LIMA), UQAC, for helping develop the experimental setup.

References

[1] T. RATVASKY, R. RANAUDO, Icing effects on aircraft stability and control determined from flight data - Preliminary results, in: 31st Aerosp. Sci. Meet., American Institute of Aeronautics and Astronautics, Reston, Virigina, 1993. https://doi.org/10.2514/6.1993-398.

[2] P. Irajizad, S. Nazifi, H. Ghasemi, Icephobic surfaces: Definition and figures of merit, Adv. Colloid Interface Sci. (2019). https://doi.org/10.1016/j.cis.2019.04.005.

[3] M.J. Kreder, J. Alvarenga, P. Kim, J. Aizenberg, Design of anti-icing surfaces: smooth, textured or slippery?, Nat. Rev. Mater. 1 (2016) 15003. https://doi.org/10.1038/natrevmats.2015.3.

[4] Y. Shen, X. Wu, J. Tao, C. Zhu, Y. Lai, Z. Chen, Icephobic materials: Fundamentals, performance evaluation, and applications, Prog. Mater. Sci. 103 (2019) 509–557. https://doi.org/10.1016/j.pmatsci.2019.03.004.

[5] P. Irajizad, S. Nazi, H. Ghasemi, Icephobic surfaces : De fi nition and fi gures of

merit, 269 (2019) 203–218. https://doi.org/10.1016/j.cis.2019.04.005.

[6] W. Hou, Y. Shen, J. Tao, Y. Xu, J. Jiang, H. Chen, Z. Jia, Anti-icing performance of the superhydrophobic surface with micro-cubic array structures fabricated by plasma etching, Colloids Surfaces A Physicochem. Eng. Asp. 586 (2020) 124180. https://doi.org/10.1016/j.colsurfa.2019.124180.

[7] L. Boinovich, A.M. Emelyanenko, V. V. Korolev, A.S. Pashinin, Effect of wettability on sessile drop freezing: When superhydrophobicity stimulates an extreme freezing delay, Langmuir. 30 (2014) 1659–1668. https://doi.org/10.1021/la403796g.

[8] G. Wang, Y. Shen, J. Tao, X. Luo, L. Zhang, Y. Xia, Fabrication of a superhydrophobic surface with a hierarchical nanoflake-micropit structure and its anti-icing properties, RSC Adv. 7 (2017) 9981–9988. https://doi.org/10.1039/c6ra28298a.

[9] Y. Qi, Z. Yang, T. Chen, Y. Xi, J. Zhang, Fabrication of superhydrophobic surface with desirable anti-icing performance based on micro/nano-structures and organosilane groups, Appl. Surf. Sci. 501 (2020) 144165. https://doi.org/10.1016/j.apsusc.2019.144165.

[10] T. Vasileiou, T.M. Schutzius, D. Poulikakos, Imparting Icephobicity with Substrate Flexibility, Langmuir. 33 (2017) 6708–6718. https://doi.org/10.1021/acs.langmuir.7b01412.

[11] G. Momen, R. Jafari, M. Farzaneh, Ice repellency behaviour of superhydrophobic surfaces: Effects of atmospheric icing conditions and surface roughness, Appl. Surf. Sci. 349 (2015) 211–218. https://doi.org/10.1016/j.apsusc.2015.04.180.

[12] A. Azimi Yancheshme, G. Momen, R. Jafari Aminabadi, Mechanisms of ice formation and propagation on superhydrophobic surfaces: A review, Adv. Colloid Interface Sci. 279 (2020) 102155. https://doi.org/10.1016/j.cis.2020.102155.

[13] E.J. Langham, B.J. Mason, The Heterogeneous and Homogeneous Nucleation of Supercooled Water, Proc. R. Soc. A Math. Phys. Eng. Sci. (1958). https://doi.org/10.1098/rspa.1958.0207.

[14] X.Y. Liu, Heterogeneous nucleation or homogeneous nucleation?, J. Chem. Phys. 112 (2000) 9949–9955. https://doi.org/10.1063/1.481644.

[15] Y. Shen, X. Xie, Y. Xie, J. Tao, J. Jiang, H. Chen, Y. Lu, Y. Xu, Statistically understanding the roles of nanostructure features in interfacial ice nucleation for enhancing icing delay performance, Phys. Chem. Chem. Phys. 21 (2019) 19785–19794. https://doi.org/10.1039/C9CP04103F.

[16] J. Jiang, G.X. Li, Q. Sheng, G.H. Tang, Microscopic mechanism of ice nucleation: The effects of surface rough structure and wettability, Appl. Surf. Sci. 510 (2020)

145520. https://doi.org/10.1016/j.apsusc.2020.145520.

[17] F.J. Montes Ruiz-Cabello, S. Bermúdez-Romero, P.F. Ibáñez-Ibáñez, M.A. Cabrerizo-Vílchez, M.A. Rodríguez-Valverde, Freezing delay of sessile drops: Probing the impact of contact angle, surface roughness and thermal conductivity, Appl. Surf. Sci. 537 (2021) 147964. https://doi.org/10.1016/j.apsusc.2020.147964.

[18] M. Rahimi, A. Afshari, E. Thormann, Effect of Aluminum Substrate Surface Modification on Wettability and Freezing Delay of Water Droplet at Subzero Temperatures, ACS Appl. Mater. Interfaces. 8 (2016) 11147–11153. https://doi.org/10.1021/acsami.6b02321.

[19] P. Hao, C. Lv, X. Zhang, Freezing of sessile water droplets on surfaces with various roughness and wettability, Appl. Phys. Lett. 104 (2014) 161609. https://doi.org/10.1063/1.4873345.

[20] Y. Wang, Z. Wang, Sessile droplet freezing on polished and micro-micro-hierarchical silicon surfaces, Appl. Therm. Eng. 137 (2018) 66–73. https://doi.org/10.1016/j.applthermaleng.2018.03.068.

[21] E.S. Gadelmawla, M.M. Koura, T.M.A. Maksoud, I.M. Elewa, H.H. Soliman, Roughness parameters, J. Mater. Process. Technol. 123 (2002) 133–145. https://doi.org/10.1016/S0924-0136(02)00060-2.

[22] T. Bartkowiak, M. Mendak, K. Mrozek, M. Wieczorowski, Analysis of surface microgeometry created by electric discharge machining, Materials (Basel). (2020). https://doi.org/10.3390/ma13173830.

[23] K. Peta, T. Bartkowiak, P. Galek, M. Mendak, Contact angle analysis of surface topographies created by electric discharge machining, Tribol. Int. (2021). https://doi.org/10.1016/j.triboint.2021.107139.

[24] N.D. Boscher, V. Vaché, P. Carminati, P. Grysan, P. Choquet, A simple and scalable approach towards the preparation of superhydrophobic surfaces-importance of the surface roughness skewness, J. Mater. Chem. A. 2 (2014) 5744–5750. https://doi.org/10.1039/c4ta00366g.

[25] W.Z. Yuan, L.Z. Zhang, Lattice Boltzmann simulation of droplets impacting on superhydrophobic surfaces with randomly distributed rough structures, Langmuir. 33 (2017) 820–829. https://doi.org/10.1021/acs.langmuir.6b04041.

[26] L.Z. Zhang, W.Z. Yuan, A lattice Boltzmann simulation of coalescence-induced droplet jumping on superhydrophobic surfaces with randomly distributed structures, Appl. Surf. Sci. 436 (2018) 172–182. https://doi.org/10.1016/j.apsusc.2017.11.200.

[27] N. Sharifi, M. Pugh, C. Moreau, A. Dolatabadi, Developing hydrophobic and superhydrophobic TiO2 coatings by plasma spraying, Surf. Coatings Technol. 289 (2016) 29–36. https://doi.org/10.1016/j.surfcoat.2016.01.029.

[28] Y.H. Yeong, E. Loth, J. Sokhey, A. Lambourne, Ice Adhesion Strength on Hydrophobic and Superhydrophobic Coatings, in: 6th AIAA Atmos. Sp. Environ. Conf., American Institute of Aeronautics and Astronautics, Reston, Virginia, 2014. https://doi.org/10.2514/6.2014-2063.

[29] A. Davis, Y.H. Yeong, A. Steele, I.S. Bayer, E. Loth, Superhydrophobic nanocomposite surface topography and ice adhesion, ACS Appl. Mater. Interfaces. 6 (2014) 9272–9279. https://doi.org/10.1021/am501640h.

[30] E. Vazirinasab, K. Maghsoudi, R. Jafari, G. Momen, A comparative study of the icephobic and self-cleaning properties of Teflon materials having different surface morphologies, J. Mater. Process. Technol. 276 (2020) 116415. https://doi.org/10.1016/j.jmatprotec.2019.116415.

[31] M. Psarski, D. Pawlak, J. Grobelny, G. Celichowski, Relationships between surface chemistry, nanotopography, wettability and ice adhesion in epoxy and SU-8 modified with fluoroalkylsilanes from the vapor phase, Appl. Surf. Sci. 479 (2019) 489–498. https://doi.org/10.1016/j.apsusc.2019.02.082.

[32] D. mname Acemoglu, P. mname Restrepo, Artificial Intelligence, Automation and Work, SSRN Electron. J. (2018). https://doi.org/10.2139/ssrn.3098384.

[33] S. Li, J. Qin, M. He, R. Paoli, Fast Evaluation of Aircraft Icing Severity Using Machine Learning Based on XGBoost, Aerospace. 7 (2020) 36. https://doi.org/10.3390/aerospace7040036.

[34] Y. Reich, S.V. Barai, Evaluating machine learning models for engineering problems, Artif. Intell. Eng. 13 (1999) 257–272. https://doi.org/10.1016/S0954-1810(98)00021-1.

[35] A. Azimi Yancheshme, S. Hassantabar, K. Maghsoudi, S. Keshavarzi, R. Jafari, G. Momen, Integration of experimental analysis and machine learning to predict drop behavior on superhydrophobic surfaces, Chem. Eng. J. 417 (2021) 127898. https://doi.org/10.1016/j.cej.2020.127898.

[36] S. Ringdahl, S. Xiao, J. He, Z. Zhang, Machine Learning Based Prediction of Nanoscale Ice Adhesion on Rough Surfaces, Coatings. 11 (2020) 33. https://doi.org/10.3390/coatings11010033.

[37] R. Ramachandran, Using neural networks to predict icephobic performance, (2020). http://arxiv.org/abs/2008.00966.

[38] M. Fitzner, P. Pedevilla, A. Michaelides, Predicting heterogeneous ice nucleation with a data-driven approach, Nat. Commun. 11 (2020) 4777. https://doi.org/10.1038/s41467-020-18605-3.

[39] K. Maghsoudi, G. Momen, R. Jafari, M. Farzaneh, Direct replication of micro-nanostructures in the fabrication of superhydrophobic silicone rubber surfaces by

compression molding, Appl. Surf. Sci. 458 (2018) 619–628. https://doi.org/10.1016/j.apsusc.2018.07.099.

[40] K. Maghsoudi, E. Vazirinasab, G. Momen, R. Jafari, Icephobicity and durability assessment of superhydrophobic surfaces: The role of surface roughness and the ice adhesion measurement technique, J. Mater. Process. Technol. 288 (2021) 116883. https://doi.org/10.1016/j.jmatprotec.2020.116883.

[41] M. Sedlaček, B. Podgornik, J. Vižintin, Correlation between standard roughness parameters skewness and kurtosis and tribological behaviour of contact surfaces, Tribol. Int. 48 (2012) 102–112. https://doi.org/10.1016/j.triboint.2011.11.008.

[42] M. Rahimi, A. Afshari, P. Fojan, L. Gurevich, The effect of surface modification on initial ice formation on aluminum surfaces, Appl. Surf. Sci. 355 (2015) 327–333. https://doi.org/10.1016/j.apsusc.2015.06.201.

[43] M.A. Rahman, A.M. Jacobi, Drainage of frost melt water from vertical brass surfaces with parallel microgrooves, Int. J. Heat Mass Transf. 55 (2012) 1596–1605. https://doi.org/10.1016/j.ijheatmasstransfer.2011.11.015.

[44] R.O. Piucco, C.J.L. Hermes, C. Melo, J.R. Barbosa, A study of frost nucleation on flat surfaces, Exp. Therm. Fluid Sci. 32 (2008) 1710–1715. https://doi.org/10.1016/j.expthermflusci.2008.06.004.

[45] G. Heydari, E. Thormann, M. Järn, E. Tyrode, P.M. Claesson, Hydrophobic Surfaces: Topography Effects on Wetting by Supercooled Water and Freezing Delay, J. Phys. Chem. C. 117 (2013) 21752–21762. https://doi.org/10.1021/jp404396m.

[46] J. Frenkel, A General Theory of Heterophase Fluctuations and Pretransition Phenomena, J. Chem. Phys. 7 (1939) 538–547. https://doi.org/10.1063/1.1750484.

[47] T.M. Schutzius, S. Jung, T. Maitra, P. Eberle, C. Antonini, C. Stamatopoulos, D. Poulikakos, Physics of Icing and Rational Design of Surfaces with Extraordinary Icephobicity, Langmuir. 31 (2015) 4807–4821. https://doi.org/10.1021/la502586a.

[48] A.M. Robin H.A. Ras, Non-wettable Surfaces: Theory, Preparation and Applications, 2016.

[49] X. Zhang, X. Liu, X. Wu, J. Min, Experimental investigation and statistical analysis of icing nucleation characteristics of sessile water droplets, Exp. Therm. Fluid Sci. 99 (2018) 26–34. https://doi.org/10.1016/j.expthermflusci.2018.07.027.

[50] F. Tancini, Y.-L. Wu, W.B. Schweizer, J.-P. Gisselbrecht, C. Boudon, P.D. Jarowski, M.T. Beels, I. Biaggio, F. Diederich, 1,1-Dicyano-4-[4-(diethylamino)phenyl]buta-1,3-dienes: Structure-Property Relationships, European J. Org. Chem. 2012 (2012) 2756–2765. https://doi.org/10.1002/ejoc.201200111.

[51] D. Turnbull, J.C. Fisher, Rate of Nucleation in Condensed Systems, J. Chem. Phys. 17 (1949) 71–73. https://doi.org/10.1063/1.1747055.

[52] B. Na, R.L. Webb, A fundamental understanding of factors affecting frost nucleation, Int. J. Heat Mass Transf. 46 (2003) 3797–3808. https://doi.org/10.1016/S0017-9310(03)00194-7.

[53] H. Li, I. V. Roisman, C. Tropea, J. Li, S. Fu, Water Drop Impact on Cold Surfaces with Solidification, in: AIP Conf. Proc., 2011: pp. 451–453. https://doi.org/10.1063/1.3651944.

[54] S. Jung, M. Dorrestijn, D. Raps, A. Das, C.M. Megaridis, D. Poulikakos, Are superhydrophobic surfaces best for icephobicity?, Langmuir. 27 (2011) 3059–3066. https://doi.org/10.1021/la104762g.

[55] Y. Bengio, Learning Deep Architectures for AI, Found. Trends® Mach. Learn. 2 (2009) 1–127. https://doi.org/10.1561/2200000006.

[56] V. Asghari, Y.F. Leung, S.-C. Hsu, Deep neural network based framework for complex correlations in engineering metrics, Adv. Eng. Informatics. 44 (2020) 101058. https://doi.org/10.1016/j.aei.2020.101058.

[57] T. Dozat, Incorporating Nesterov Momentum into Adam, ICLR Work. (2016) 2013–2016.

[58] S. Lundberg, S.-I. Lee, A Unified Approach to Interpreting Model Predictions, Adv. Neural Inf. Process. Syst. 2017–Decem (2017) 4766–4775. http://arxiv.org/abs/1705.07874.